https://doi.org/10.5194/egusphere-2024-2014
Preprint. Discussion started: 12 July 2024

Land use change influence on atmospheric organic gases, aerosols, and radiative effects

Ryan Vella[1,2], Matthew Forrest[3], Andrea Pozzer[1,4], Alexandra P. Tsimpidi[5], Thomas Hickler[3,6], Jos Lelieveld[1,4], and Holger Tost[2]

[1]Atmospheric Chemistry Department, Max Planck Institute for Chemistry, Mainz, Germany
[2]Institute for Atmospheric Physics, Johannes Gutenberg University Mainz, Mainz, Germany
[3]Senckenberg Biodiversity and Climate Research Centre (SBiK-F), Frankfurt am Main, Germany
[4]Climate and Atmosphere Research Center, The Cyprus Institute, Nicosia, Cyprus
[5]Institute for Energy and Climate Research, IEK-8: Troposphere, Forschungszentrum Jülich GmbH, Jülich, Germany
[6]Department of Physical Geography, Goethe University, Frankfurt am Main, Germany

Correspondence: Ryan Vella (ryan.vella@mpic.de)

Abstract.

Biogenic volatile organic compounds (BVOC) are emitted in large quantities from the terrestrial biosphere and play a significant role in atmospheric gaseous and aerosol composition. Such emissions account for 90% of the total global volatile organic compound (VOC) emissions and exert a significant influence on the atmosphere's oxidation capacity. BVOCs are precursors of secondary organic aerosols (SOA), which affect the radiation budget both directly through scattering and absorption of sunlight and indirectly through modifying cloud formation, properties and distribution. Human activities have extensively altered natural vegetation cover, primarily by converting forests into agricultural land. In this work, a global atmospheric chemistry-climate model with interactive vegetation was employed to study the impacts of perturbing the biosphere through human land use change, consequently exploring changes in BVOC emissions and atmospheric aerosol burden. Given that our vegetation model simulates potential natural vegetation (PNV), a land use scheme was implemented to constrain the Tree Plant Functional Type (PFT) cover based on land transformation fraction maps from the year 2015. Two scenarios are evaluated: (1) comparing present-day land cover, which includes areas deforested for crops and grazing land, with the natural vegetation cover (PNV), and (2) an extreme reforestation scenario where present-day crop and grazing land are restored to natural vegetation. We find that, compared to the PNV scenario, present-day deforestation results in a 26% reduction in BVOC emissions, which decreases the global biogenic SOA (bSOA) burden by 0.16 Tg (a decrease of 29%), while the total organic aerosol (OA) burden decreases by 0.17 Tg (a reduction of 9%). On the other hand, the extreme reforestation scenario, compared to present-day land cover, suggests an increase in BVOC emissions by 22%, which increases the bSOA by 0.11 Tg and total OA burden by 0.12 Tg, an increase of 26% and 6%, respectively. The assessment includes changes in the cloud condensation nuclei (CCN) and cloud droplet number concentration (CDNC) in each scenario. In the present-day deforestation scenario, we estimate a positive total radiative effect (aerosol + cloud) of 60.4 mW m^{-2} (warming) compared with the natural vegetation scenario, while in the extreme reforestation scenario, we report a negative effect (cooling) of 38.2 mW m^{-2} compared to the PNV scenario.

https://doi.org/10.5194/egusphere-2024-2014
Preprint. Discussion started: 12 July 2024

1 Introduction

Human activities have significantly modified the natural vegetation cover, primarily through the conversion of forests into agricultural land. It is estimated that approximately half of the Earth's land surface has been affected by human activities (Hurtt et al., 2011). Land cover change (LCC) has a substantial impact on the Earth system as the biosphere plays a central role in major biophysical and biogeochemical cycles, as well as feedbacks with the atmosphere (Bonan, 2008). Forests store 45% of terrestrial carbon and can sequester large amounts of carbon (Field and Raupach, 2004). Furthermore, forests play a significant role in sustaining the hydrological cycle through evapotranspiration, which influences cloud formation, the onset of precipitation, and consequently surface temperatures (Betts et al., 2004; Vicente-Serrano et al., 2015). Land cover plays a crucial role in surface albedo, with dense forests capable of absorbing up to 90% of solar radiation (Forster et al., 2007a). In high latitudes, forests can mask the high albedo of snow, leading to planetary warming through increased solar heating of the land (Bonan, 2008).

The terrestrial biosphere is also the primary source of biogenic volatile organic compounds (BVOCs) emissions such as isoprene and various terpenes, accounting for around 90% of the total VOC emissions to the atmosphere (Guenther et al., 1995). Reported global isoprene emissions, the primary BVOC, span 412 to 682 Tg yr^{-1} (e.g., Sindelarova et al., 2014; Guenther et al., 2006; Vella et al., 2023a). BVOCs are highly reactive and short-lived, with lifetimes typically ranging from minutes to hours. Upon emission, they rapidly interact with tropospheric oxidant gases, thereby exerting a substantial influence on the oxidation capacity of the atmosphere (Lelieveld et al., 2008; Atkinson, 2000; Atkinson and Arey, 2003).

The short lifespan of BVOCs stems from their rapid oxidation upon release from the canopy. This oxidation primarily involves the OH radical as well as other key oxidizing agents like O_3 and NO_3 radicals (Shrivastava et al., 2017). These reactions produce various lower volatility oxidation products that tend to partition into the aerosol phase, leading to the formation of biogenic secondary organic aerosols (bSOA) (Kavouras et al., 1998; Spracklen et al., 2011). Isoprene-derived oxidation products mainly contribute to the condensation onto existing aerosols, whereas the oxidation products from monoterpenes, despite being less abundant compared to isoprene, play a crucial role in generating new particles, thus influencing SOA formation significantly (Jokinen et al., 2015). When biogenic SOA particles reach a dry radius of approximately 50 nm, they contribute to the aerosol fraction involved in climate interactions. In other words, bSOA participates in the absorption and scattering of solar short-wave radiation (direct effect) and acts as condensation nuclei modifying cloud properties such as albedo and lifetime (indirect effect) (Forster et al., 2007b).

BVOC emission rates are inherently linked to land cover, and LCC can ultimately affect the climate system by influencing short-lived climate forcers like aerosols (Scott et al., 2014). In this study, we investigate the changes in BVOC emissions following crop and grazing land expansion on potential natural vegetation (PNV). We use the chemistry-climate model EMAC coupled with the global dynamic vegetation model (GDVM) LPJ-GUESS which simulates PNV. We applied a deforestation routine in LPJ-GUESS where crop and grazing land area is systematically deforested based on 2015 land cover data. Here, we present changes in BVOC emissions as well as the aerosol burden and radiation impacts using advanced descriptions in EMAC including dynamic vegetation representations that respond to changes in atmospheric states.

https://doi.org/10.5194/egusphere-2024-2014
Preprint. Discussion started: 12 July 2024

2 Model description and methods

2.1 The EMAC modelling system

The EMAC (ECHAM/MESSy Atmospheric Chemistry) model is a numerical chemistry and climate modelling system that contains submodels that represent tropospheric and middle atmospheric processes, as well as their interactions with oceans, land, and anthropogenic activities. It originally combined the ECHAM atmospheric general circulation model (GCM) (Roeckner et al., 2006) with the Modular Earth Submodel System (MESSy) (Jöckel et al., 2005) framework and philosophy, modularising physical processes as well as most of the infrastructure into submodels that can be further developed to improve existing process representations; new submodels can also be added to represent new or alternative process representations.

The configuration of the chemistry submodels in this study closely follows the approach outlined in Jöckel et al. (2016), but include aerosol processes for tropospheric applications. Aerosols are treated using the submodel GMXe (Pringle et al., 2010), where aerosol microphysics are characterised by seven interactive lognormal modes that span the typical size range of aerosol species. These modes are further categorised into four hydrophilic (nucleation, Aitken, accumulation, and coarse) and three hydrophobic (Aitken, accumulation, and coarse) aerosol modes. The representation of all aerosols assumes spherical particles. The properties of aerosols in each mode are fully determined by factors such as total mass (internal mixture of contributing species), density, number concentration, median radius, and width of the lognormal distribution. After each simulation step aerosols may transfer between modes depending on size changes.

Organic aerosol species are additionally described by the Organic Aerosol Composition and Evolution (ORACLE) submodel (Tsimpidi et al., 2014), taking into account the partitioning between aerosols and the gas phase based on the volatility basis set (VBS) framework (Donahue et al., 2006). ORACLE describes the following organic aerosols (OA): Secondary organic aerosols from the oxidation of anthropogenic (aSOA) and biogenic (bSOA) VOCs; primary organic aerosols from emissions from fossil fuel and bio-fuel combustion (fPOA) and biomass burning (bbPOA); and secondary organic aerosols from their subsequent photochemical oxidation (fSOA and bbSOA, respectively) (Tsimpidi et al., 2016, 2017). The submodel employs a simple photochemical ageing scheme that effectively models the combined impacts of fragmentation and functionalisation of organic compounds. The module not only predicts the mass concentration of organic aerosol (OA) components but also predicts their oxidation state (expressed as O : C), enabling their categorisation into primary OA (POA, chemically unprocessed), freshly formed secondary OA (SOA, with low oxygen content), and aged SOA (highly oxygenated). By explicitly simulating the chemical conversion of OA from initial emissions to a highly oxygenated state during photochemical ageing, ORACLE facilitates tracking changes in OA hygroscopicity resulting from these reactions. This allows the computation of OA particle capability to serve as cloud condensation nuclei. Details on the implementation of ORACLE (v2.0) in EMAC, including an evaluation of the model, could be found in Tsimpidi et al. (2018). The output from the ORACLE model, based on the described setup, has been compared with observational data in tropical regions. It was found that ORACLE provides OA surface concentrations within 60% of the observed values, as documented in several studies (Hewitt et al., 2010; de Sá et al., 2019; Chen et al., 2009; Schmale et al., 2013; Tiitta et al., 2014; Zhang et al., 2010).

https://doi.org/10.5194/egusphere-2024-2014
Preprint. Discussion started: 12 July 2024

Heterogeneous and gas-phase chemistry are treated through the MECCA submodel (Sander et al., 2019), employing the Mainz Isoprene Mechanism (MIM1) as the chemical mechanism (Pöschl et al., 2000; Jöckel et al., 2006), which includes over 100 gas-phase species and more than 250 reactions. Dry deposition, sedimentation, and wet deposition processes are simulated using the submodules DDEP, SEDI (both Kerkweg et al., 2006) , and SCAV (Tost et al., 2006a), respectively. Within this framework, convective cloud processes are taken into account based on the approach proposed by Tost et al. (2006b), utilising the convection schemes from Tiedtke (1989) and Nordeng (1994). However, convective cloud microphysics is solely based on temperature and moisture profiles, without accounting for the influence of aerosols on liquid droplet or ice formation processes. The vertical velocity distribution used for aerosol activation by grid-scale clouds in EMAC is calculated as the sum of the grid mean vertical velocity and the turbulent contribution, as detailed by Brinkop and Roeckner (1995). Large-scale stratiform clouds are described by the CLOUD submodel, which, in the applied configuration, incorporates a two-moment cloud microphysics scheme for cloud droplets and ice crystals, as detailed by Lohmann et al. (1999, 2007); Lohmann and Ferrachat (2010) and Lohmann and Kärcher (2002). CLOUD solves prognostic equations for specific humidity, liquid cloud mixing ratio, ice cloud mixing ratio, cloud droplet number concentration (CDNC), and ice crystal number concentration (ICNC).

CLOUD incorporates a prognostic cloud droplet nucleation process to represent aerosol-cloud interactions in large-scale clouds (excluding convective warm clouds) using aerosol information provided by GMXe. This prognostic nucleation scheme is based on the aerosol activation parameterisation proposed by Abdul-Razzak and Ghan (2000) and employs the κ-Köhler method (Petters and Kreidenweis, 2007) to calculate aerosol hygroscopicity and critical supersaturation. This routine provides values for the parameter κ and the cloud condensation nuclei (CCN) number concentration at 0.2% and 0.4% supersaturation for each aerosol size mode (Pringle et al., 2010). The resulting CCN concentrations are then utilised in the two-moment cloud scheme described above, effectively impacting cloud properties (i.e., CDNC).

For the evaluation of the radiative effects from clouds and aerosols, we employ the methods from Ghan (2013). The calculation of the net radiative effect from aerosol-radiation interactions (RE_{ari}) involves determining the difference between the net top-of-the-atmosphere shortwave radiative flux (F) and the radiative flux, excluding the scattering and absorption of solar radiation by the aerosols (F_{clean}). F_{clean} is computed in a separate radiation call within the radiation submodel RAD. Similarly, the radiative effect from aerosol-cloud interactions (RE_{aci}) is derived by assessing the difference between F_{clean} and the flux that disregards the scattering and absorption caused by both clouds and aerosols ($F_{clear\text{-}sky,\ clean}$).

LPJ-GUESS

The Lund-Potsdam-Jena General Ecosystem Simulator (LPJ-GUESS) (Smith et al., 2001, 2014) is a dynamic global vegetation model (DGVM) featuring an individual-based model of vegetation dynamics. These dynamics are simulated as the emergent outcome of plant growth and competition for light, space, and soil resources among woody plant individuals and a herbaceous understorey in each of a number (50 in this study) of replicate patches representing random samples of each simulated locality or grid cell. The simulated plants are classified into 12 plant functional types (PFTs) discriminated by growth

https://doi.org/10.5194/egusphere-2024-2014
Preprint. Discussion started: 12 July 2024

form, phenology, photosynthetic pathway (C3 or C4), bioclimatic limits for establishment and survival and, for woody PFTs, allometry and life history strategy. LPJ-GUESS has previously been implemented in global ESMs (e.g., Weiss et al., 2014; Alessandri et al., 2017), and, more recently, coupled with EMAC (Forrest et al., 2020; Vella et al., 2023a). The LPJ-GUESS version used in this study (v4.0) currently provides information on potential natural vegetation (PNV), and it does not incorporate changes in land use. In this work, however, a custom deforestation routine was integrated to constrain the PNV using deforestation maps. The deforestation maps consist of values from 0 to 1, where a value of 1 signifies complete deforestation within the respective grid cell. The routine kills the tree PFTs after every simulated year and inhibits trees from establishing in the specified areas. This implementation allows us to constrain the vegetation cover and address the research questions presented in this work. However, the latest version of LPJ-GUESS (v4.1) features a more advanced land cover scheme, which will be incorporated into our current LPJ-GUESS version in future developments.

2.2 EMAC/LPJ-GUESS configuration

In this work, we use the standard EMAC/LPJ-GUESS coupled configuration, where the vegetation in LPJ-GUESS is entirely determined by the EMAC atmospheric state, soil type, N deposition, and fluxes (Forrest et al., 2020), but there is no feedback from the vegetation to climate variables (e.g., changes in albedo and roughness length). After each simulation day, EMAC computes the average daily values of 2-meter temperature, net downwards shortwave radiation, and total precipitation and passes these state variables to LPJ-GUESS. Vegetation information (leaf area index, foliar density, leaf area density distribution, and PFT fractional coverage) from LPJ-GUESS is then fed back to EMAC for the calculation of BVOC emission fluxes using EMAC's BVOC submodules. In this study, the BVOC fluxes in EMAC are calculated using the Model of Emissions of Gases and Aerosols from Nature (MEGAN) version 2.04 (Guenther et al., 2006).

MEGAN is based on the work of Guenther et al. (1993, 1995), where the BVOC emission flux is calculated as a function of PFT-specific emission factors, and non-dimensional activity factors. These activity factors consider sensitivities to the canopy environment, including parameters such as leaf area index (LAI), temperature, light, and leaf age. Notably, the current setup does not incorporate sensitivity to soil moisture. The parameterised canopy environment emission activity (PCEEA) algorithm is used, rather than the alternative detailed canopy environment model that calculates light and temperature at each canopy depth. The PCEEA algorithm calculates the light sensitivity within the canopy as a function of the daily average above-canopy photosynthetic photon flux density (PPFD), the solar angle and a non-dimensional factor describing the PPFD transmission through the canopy. This setup activates BVOC-aerosol-vegetation feedbacks, making vegetation and BVOC emissions sensitive to changes in temperature and above-canopy radiation (excluding diffused radiation) resulting from aerosol interactions. BVOC emissions from this model setup were evaluated and applied in other studies (e.g. Vella et al., 2023a, b).

2.3 Experimental design

The deforestation scenarios were derived from the History database of the Global Environment (HYDE v3.2) (Klein Goldewijk et al., 2017). HYDE provides a wide range of land use products, encompassing both historical and projected data. To ensure an accurate representation, we rely on HYDE's "cropland" and "grazing land" products from 2015, derived from high-resolution

https://doi.org/10.5194/egusphere-2024-2014
Preprint. Discussion started: 12 July 2024

satellite data. These products were transformed into deforestation fraction maps (Fig. 1) to constrain the vegetation in the model. Three experiments were conducted to assess the impact of human-induced deforestation on the natural land biosphere and atmospheric composition. The initial model run used simulated PNV without any deforestation. Additionally, two more model runs were conducted, incorporating deforestation. The first scenario aimed to represent present-day deforestation levels and employed deforestation based on cropland and grazing land. This scenario is referred to as "Deforested Crop and Grazing Land" (DCGL) - Fig. 1a. DCGL will sometimes be referred to as "present-day deforestation" scenario. The second scenario involved deforestation exclusively on cropland and is referred to as "Deforested Crop Land" (DCL) (Fig. 1b). We use the DCL scenario to evaluate the potential impact of restoring all grazing land back to its natural state, essentially creating an extreme afforestation scenario, while maintaining the present-day croplands for agricultural food production.

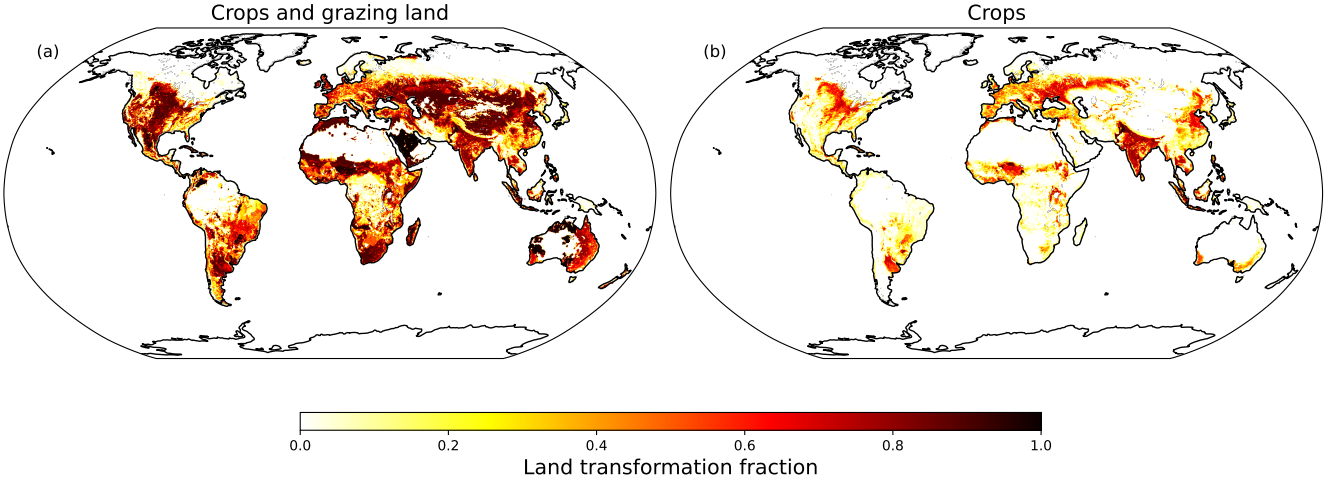

Figure 1. Deforestation maps used for the deforesting tree PFT's in LPJ-GUESS. Products derived from HYDE v3.2 based on the year 2015.

All simulations were conducted over 12 years, with the initial 2 years excluded from the analysis to ensure proper spinup and equilibrium state in the analysed data. The vegetation initial states for all simulations were taken from a previous non-chemistry 50-year run under similar atmospheric states. For this study, the simulations were performed in T63L31 resolution, i.e., approximately 1.9°× 1.9°(or approx. 180 × 180 km at the Equator) with 31 vertical levels. The meteorological fields were nudged in the troposphere towards ERA-Interim reanalysis data (Dee et al., 2011) for the respective years 2000-2012. The corresponding forcing at the sea surface (Sea Surface Temperatures (SSTs) and Sea Ice Coverages (SICs)) is also inferred from the nudging data with continuous variation. Tracers were initialized using climatological data from previous simulations spanning 2000 to 2020, while the CO_2 concentrations in the radiation and vegetation schemes were kept fixed at 384 ppmv, representing the year 2015. All simulations employ surface offline emissions, based on the year 2015 forming a consistent set of boundary conditions.

https://doi.org/10.5194/egusphere-2024-2014
Preprint. Discussion started: 12 July 2024

3 Results

3.1 Present-day land cover

This section explores changes in the natural land biosphere caused by human deforestation for crops and grazing land, based on 2015 HYDE land use data. We demonstrate how these alterations in the biosphere propagate to the atmosphere, affecting BVOC surface fluxes and impacting aerosol burden and other atmospheric states.

3.1.1 Changes in vegetation states

Fig. 2 shows the PNV scenario's spatial distribution of the vegetation fraction for tree (a,c) and grass (b,d) PFTs. As illustrated in Fig. 2c, the deforestation routine implemented in LPJ-GUESS effectively prevents tree establishment in the transformed regions outlined in Fig. 1a, resulting in the dominance of grass PFTs in these areas (Fig. 2d). Present-day deforestation decreases the global tree coverage by 1026 Megahectares (Mha), while it expands the grass coverage by 953 Mha. We find that the global carbon biomass, defined as the amount of functional tissue in land vegetation (including roots), decreases from 567 PgC in the PNV scenario to 503 PgC in the DCGL scenario. This indicates that the present-day land biosphere has lost 64 PgC compared to natural vegetation (Fig. S1 in the supplementary material).

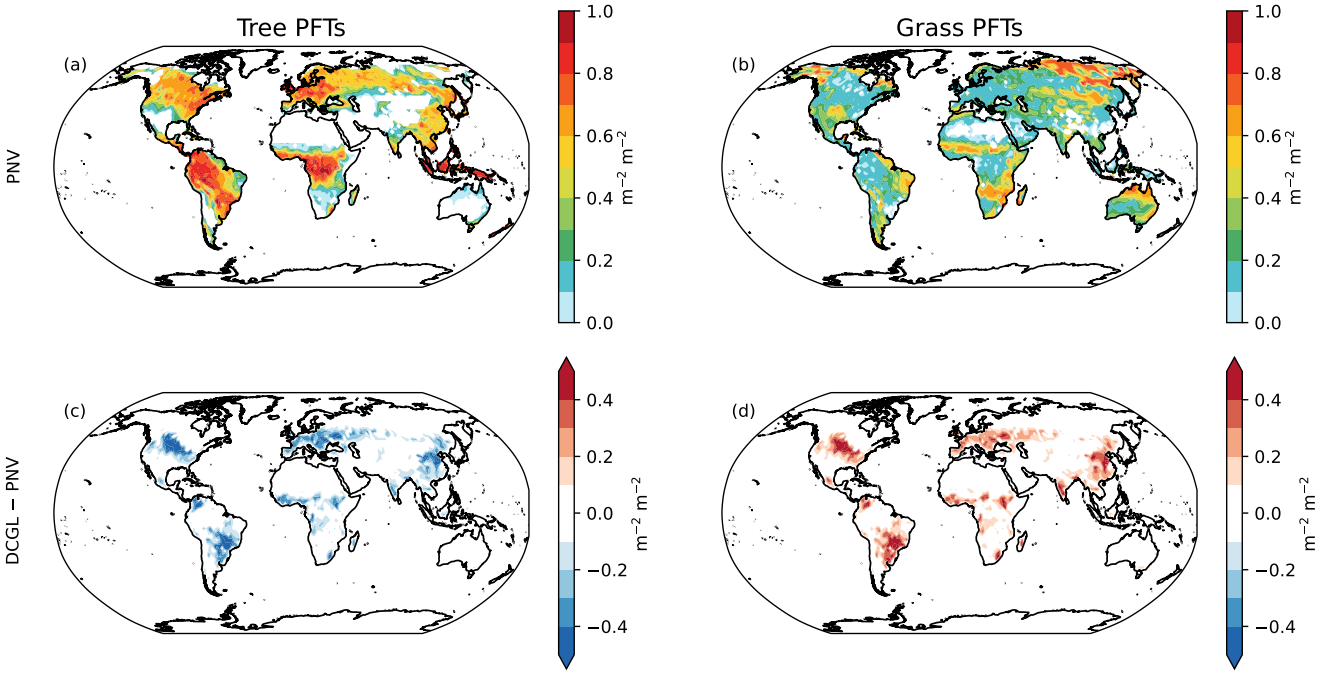

Figure 2. Changes in the tree and grass cover fractions (area of vegetation per unit ground area). The right panels show the tree PFTs while the left panels show grass PFTs. Panels a-b show the global distribution of the vegetation fraction in the PNV scenario. Panels c-d show the changes from the deforestation (DCGL−PNV) scenario.

https://doi.org/10.5194/egusphere-2024-2014
Preprint. Discussion started: 12 July 2024

3.1.2 BVOC surface emissions

The clearing of biomass from deforestation practices impacts the BVOC global emissions. Fig. 3 a-b shows the surface isoprene and monoterpene emissions in the PNV scenario. The model simulates fluxes of up to 100 g(C) m^{-2} day^{-1} of isoprene, and 8 g(C) m^{-2} day^{-1} of monoterpene in the tropics. Fig. c-d shows the spatial changes in the BVOC fluxes resulting from deforestation.

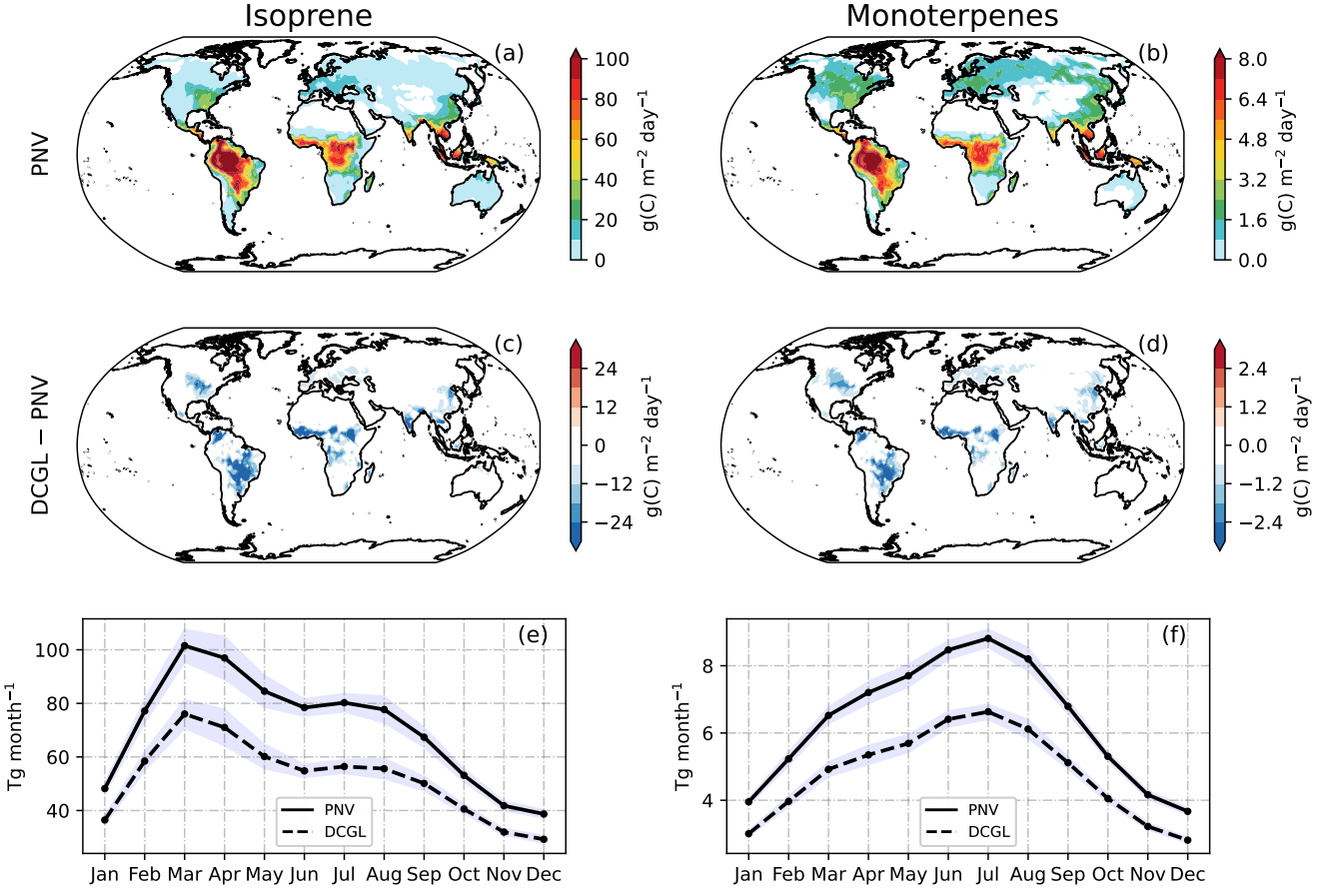

Figure 3. Isoprene and monoterpene surface fluxes for the PNV scenario (a-b). Subplots c and d show the spatial difference in isoprene and monoterpene emission fluxes (DCGL − PNV). Monthly emissions based on the 10-year average for isoprene (e) and monoterpenes (f). The shading represents 1 standard deviation derived from the monthly averages based on 10 simulated years. Fluxes in the Southern Hemisphere were shifted by 6 months to juxtapose the seasonal cycle.

In Fig. 3e-f, the temporal profile of global monthly emission totals is depicted, with shading indicating 1-σ variability based on 10 simulated years. To capture the true seasonal cyclea, values from the Southern Hemisphere were shifted by 6 months before combining fluxes from both hemispheres. In the PNV scenario, the global annual emission flux for isoprene totalled

https://doi.org/10.5194/egusphere-2024-2014
Preprint. Discussion started: 12 July 2024

845.7 Tg, which decreased to 620.9 Tg in the DCGL scenario, marking a reduction of 224.8 Tg (a 27% decrease relative to PNV). Similarly, for monoterpenes, the annual global emissions in PNV were 76.0 Tg and 57.3 Tg in DCGL, respectively, indicating a decrease of 18.7 Tg (a 25% decrease relative to PNV). Consequently, the global, annual source of BVOCs decreases by 243.5 Tg.

3.1.3 Aerosol burden, cloud interactions, and radiative effects

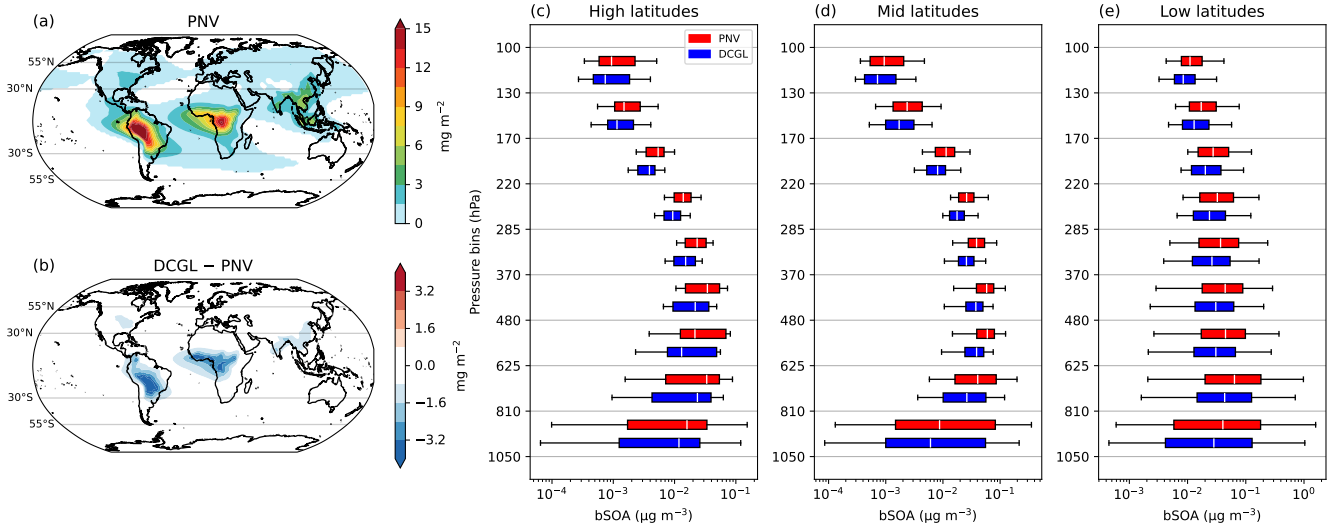

Figure 4. Total column bSOA from PNV (a) and changes in bSOA from deforestation (DCGL − PNV) (b). Panels (c), (d), and (e) show the vertical profiles of bSOA, represented by box-whisker plots for different pressure bins. The white line marks the median, the box corresponds to the lower and upper quarterlies, and the whiskers represent the 5th–95th percentile. The latitude ranges are defined as follows: High latitudes (90–55°S and 55–90°N), mid-latitudes (55–30°S and 30–55°N), and low latitudes (30°S–30°N). A log scale is used for the x-axis of (c), (d), (e).

Fig. 4 illustrates the bSOA burden, including the total column burden for the PNV depicted in Fig. 4a, as well as changes in the column burden resulting from deforestation (4b), and, the vertical profiles across three latitude bands (4c-e). The vertical profile is represented using box-whisker plots, showcasing variations at different pressure bins. In the PNV scenario, the bSOA load exhibits its highest concentration over the Amazon forest and the Congo basin, reaching a column mass of up to 15 mg m^{-2}. In the PNV scenario, we estimate a total annual OA atmospheric burden of 1.87 Tg, of which 0.56 Tg are bSOA, while in DCGL the total annual OA atmospheric burden reduces to 1.70 Tg, of which 0.40 Tg are bSOA. The bSOA burden decreased by 29% while the total OA decreased by 9%.

https://doi.org/10.5194/egusphere-2024-2014
Preprint. Discussion started: 12 July 2024

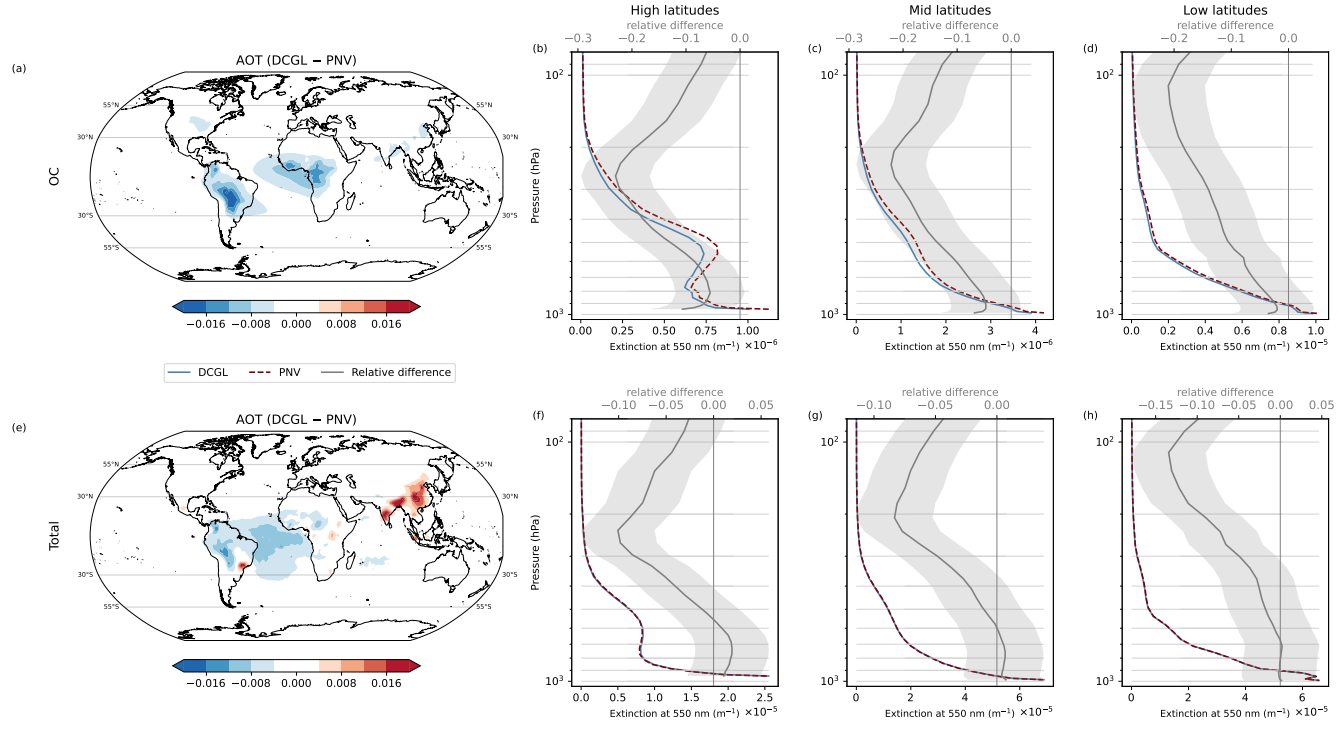

Figure 5. Spatial maps of the total column aerosol optical thickness (AOT) at 550 nm for organic carbon (OC) (a), and total aerosol (e). Vertical profiles for the aerosol extinction at 550 nm for DCGL, PNV, along with the relative differences ((DCGL−PNV)/PNV) in different latitude bands. Organic aerosol in (b), (c), (d), and total aerosol in (f), (g), (h). The latitude ranges are defined as follows: High latitudes (90–55°S and 55–90°N), mid-latitudes (55–30°S and 30–55°N), and low latitudes (30°S–30°N).The grey area represents 1 standard deviation of the spatio–temporal mean (grey line). Please note the different scales for the relative differences.

Fig. 5 shows changes in the total column aerosol optical thickness (AOT) and extinction at 550 nm for OA (top panels) and for the total aerosols (bottom panels). The aerosol extinction refers to the fractional depletion of radiance per unit path length (m^{-1}). The aerosol optical thickness (AOT) is determined by integrating the aerosol extinction over the full atmospheric column, making it a dimensionless quantity. Fig. 5a illustrates the absolute changes in AOT from organic carbon (OC) and suggests a decrease of up to 0.02 over the Amazon forest and Congo basin in Africa. Panels b, c and, d, show a consistent decrease in the OC extinction, with the highest relative difference peaking at around 250 hPa in the high and mid-latitudes, and around 100 hPa in the tropics. Our calculations indicate a global decrease in the OC AOT of -7%, with corresponding decreases of -10%, -9%, and -5% in high, mid, and low latitudes. EMAC simulates the optical properties of six aerosol species, namely organic carbon (OC), black carbon (BC), water-soluble inorganic aerosols (WASO), dust (DU), sea salt (SS), and aerosol-associated water (H2O). The aerosol extinction at 550 nm from the total aerosol suggests a decrease over the tropics (Fig. 5e), however, this trend varies significantly across latitudinal bands. Notably, there is a marginal increase of 0.1% in the high latitudes with declines of -0.5% and -0.6% in mid and low latitudes, respectively.

https://doi.org/10.5194/egusphere-2024-2014
Preprint. Discussion started: 12 July 2024

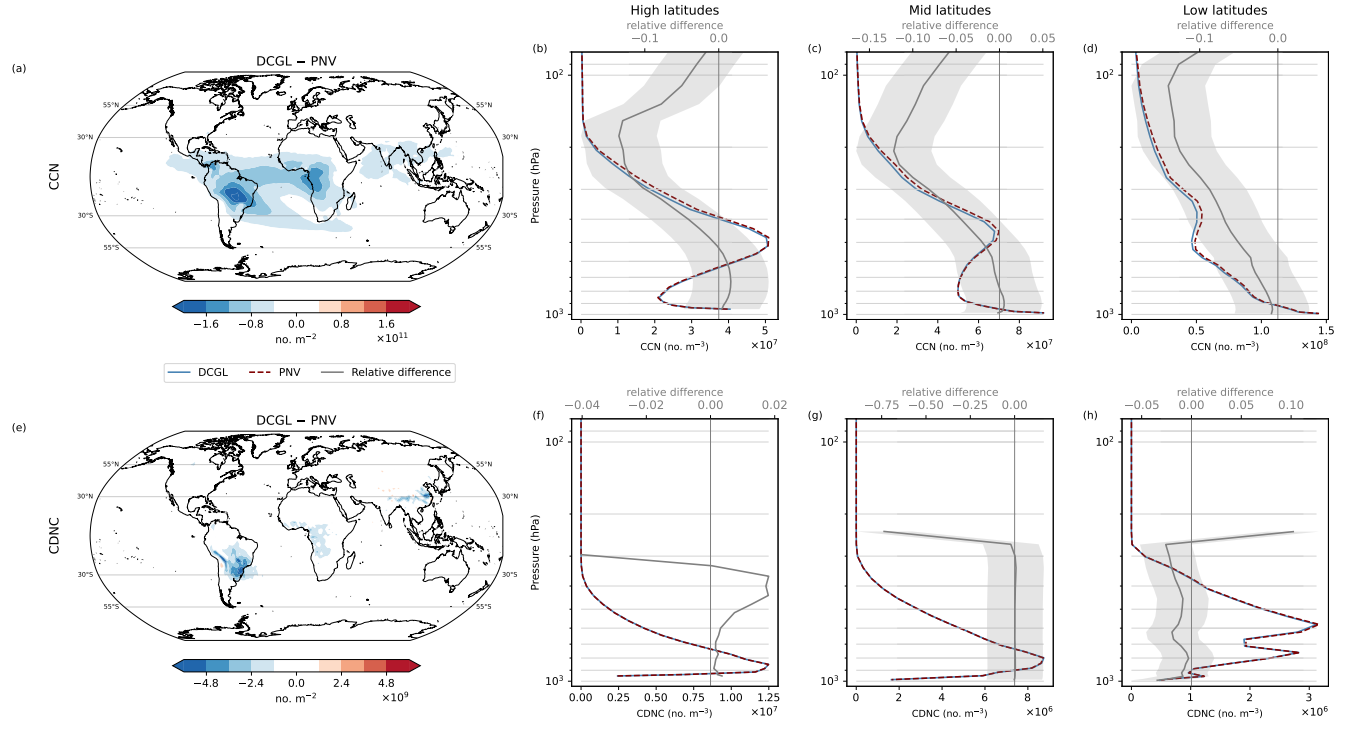

Figure 6. Changes in cloud condensation nuclei (CCN) at 0.2% supersaturation (top panels) and cloud droplet number concentration (CDNC) (bottom panels). The panels on the left-hand side, (a) and (e), show the spatial difference in the total column burden (number of particles per square meter), for CCN and CDNC, respectively, emerging from DCGL compared to natural vegetation (DCGL − PNV). The panels on the right-hand side show the total-column vertical profiles from DCGL and PNV simulations and their relative difference are shown. Figure details are the same as Fig. 5.

Fig. 6 illustrates changes in the CCN at 0.2% supersaturation and CDNC. The reduced aerosol burden in DCGL leads to a CCN decrease of up to 2×10^{11} particles per m^2 over the tropical regions. Our calculations suggest a global decrease in CCN of 4.8%, with respective declines of 3%, 5%, and 5% in high, mid, and low latitudes, respectively. Panels (b), (c), and (d) show the vertical profile of CCN for both DCGL and PNV. In high and mid-latitudes, the difference in CCN concentration peaks around 200 hPa, showing a decrease of approximately 12% in the DCGL scenario. In the tropics, the peak difference occurs higher up in the atmosphere (around 950 hPa), also with a decrease of around 12%.

Our results indicate that the lower availability of CCN (Fig. 6a) induces a decrease in CDNC in South America, Central Africa and Eastern China. Globally, deforestation leads to a decrease of 0.2% in CDNC. Spatial averages over high and mid-latitudes suggest a general increase of 0.2% and 0.3%, respectively. Conversely, over the tropics, CDNC decreases by 0.6%. Panels (f), (g), and (h), displaying the vertical profile of CDNC, affirm that the strongest influence on CDNC, with a consistent reduction over the full column, occurs in the tropics. This suggests that the shifts in aerosol loading directly impact cloud

https://doi.org/10.5194/egusphere-2024-2014
Preprint. Discussion started: 12 July 2024

properties, particularly near the perturbed organic aerosols originating from the BVOC precursors, however, the effect appears to be small.

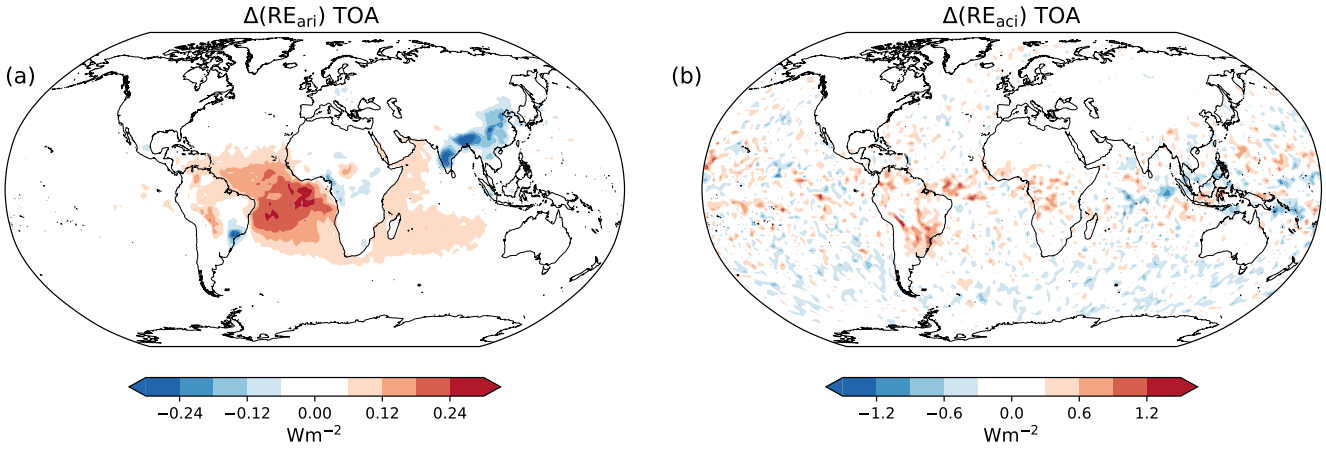

Figure 7. Aerosol and cloud radiative effect mediated by aerosol changes from deforestation (DCGL−PNV). Panels a and b show the top-of-the-atmosphere (TOA) direct (aerosol) and indirect (cloud) radiative effect, respectively.

We estimate a global increase in aerosol radiative effect (RE_{ari}) of 60.4 mW m^{-2}, the tropics experiencing a particularly pronounced increase, averaging at 91.2 mW m^{-2}. The model indicates a less prominent signal in cloud radiative effect (RE_{aci}), with a noticeable uptick of +27.5 mW m^{-2} over the tropics, but a minor global cooling effect of −8.7 mW m^{-2}. Fig. S6 in the supplementary material include maps with relative changes in bSOA, AOT, CCN, CDNC, and RE resulting from present-day land use cover compared to natural vegetation cover.

3.2 Grazing land restoration

In this section, we evaluate the changes resulting from the restoration of all grazing land to natural vegetation. In Section 3.1, PNV was used as the baseline scenario to assess changes from present-day land use cover (DCGL). In this following section, DCGL serves as the baseline scenario, with the sensitivity run being the DCL with only deforested crop cultivation, as shown in Fig. 1b. These analyses therefore represent an extreme reforestation scenario.

3.2.1 Changes in vegetation and BVOC emissions

In this scenario, where it is assumed that all grazing land is restored to natural vegetation (DCGL−DCL), the global tree cover increases by 600 Mha compared to present-day land use cover (Fig. S2 in the supplementary material). We also find that in this scenario, the global biomass increases to 546 PgC, which is an increase of 43 PgC compared to present-day land cover. Fig. S1 in the supplementary material shows the spatial distribution of biomass per unit land area and the shifts resulting from the land use scenarios considered here.

https://doi.org/10.5194/egusphere-2024-2014
Preprint. Discussion started: 12 July 2024

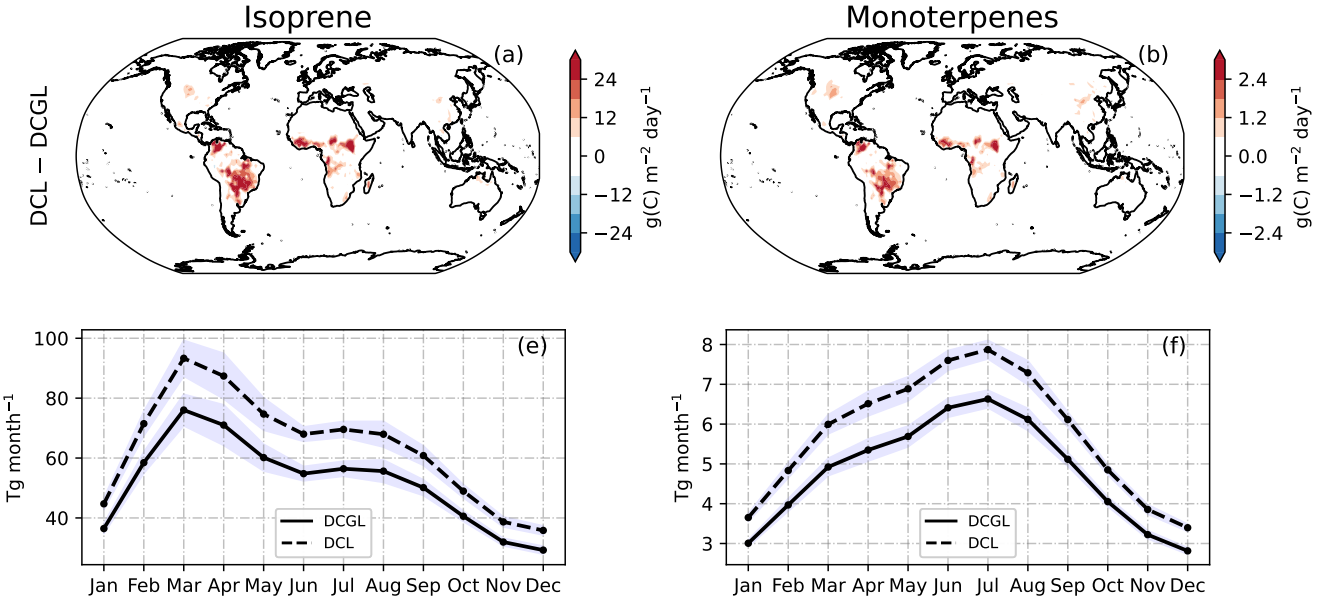

Figure 8. Spatial difference in isoprene and monoterpene emission fluxes (DCL−DCGL) (a-b). Monthly emissions based on the 10-year average for isoprene (c) and monoterpenes (d). The shading represents 1 standard deviation derived from the monthly averages based on 10 simulated years. Fluxes in the Southern Hemisphere were shifted by 6 months to conserve the seasonal cycle.

Fig. 8 depicts the changes in surface isoprene and monoterpene emissions from the grazing land restoration run compared to present-day land cover. These emission changes align with the alterations in vegetation cover (Fig. S2). Globally, annual isoprene emissions in the DCL scenario increase by 140.4 Tg (+23%) relative to the DCGL scenario, while monoterpene emissions increase by 11.6 Tg (+20%).

3.2.2 Changes in atmospheric states

The column mass of bSOA experiences a notable rise of over 3 mg m^{-2} across tropical South America and Central Africa (Fig. S3b). This rise increases the bSOA burden from 0.40 Tg in the baseline scenario to 0.50 Tg (+0.10 Tg, +25.7%), consequently perturbing the total OA burden, which increases from 1.70 Tg to 1.80 Tg (+0.11 Tg, +6.3%). Fig. S3 in the supplementary material includes the vertical bSOA profiles at the three latitude bands. The global mean OC AOT at 550 nm increases by 3.8%, with corresponding increases of 5.5%, 5%, and 2.4% in high, mid, and low latitudes, respectively. The global mean AOT at 550 nm from the total aerosols increases by 0.3%, with a corresponding decrease of 0.1% in the high latitudes and an increase of 0.4% in both mid and low latitudes. Spatial maps of the AOT and extinction vertical profiles for the different latitude bands are shown in Fig. S4.

In this scenario, we estimate a global increase in CCN of 3.5%, with increases of 2.5%, 3.7%, and 3.7% in high, mid, and low latitudes, respectively. CDNC increases globally by 0.2%, with decreases of 0.1% in high and mid-latitudes, and an increase of 0.5% in the tropics. Spatial maps and vertical profiles for the different latitude bands for CCN and CDNC can be

https://doi.org/10.5194/egusphere-2024-2014
Preprint. Discussion started: 12 July 2024

found in Fig. S5 of the supplementary material. The global aerosol direct radiative effect (RE_{ari}) is -38.2 mW m^{-2}, while the radiative effect from changes in cloud properties (RE_{aci}) is found to be +1.6 mW m^{-2} which is less than 1% and considered to be insignificant. Fig. 9 summarises the changes in atmospheric states following the conversion of grazing land to reforestation (DCL − DCGL) including radiative effects from aerosols and cloud properties (Fig. 9e-f).

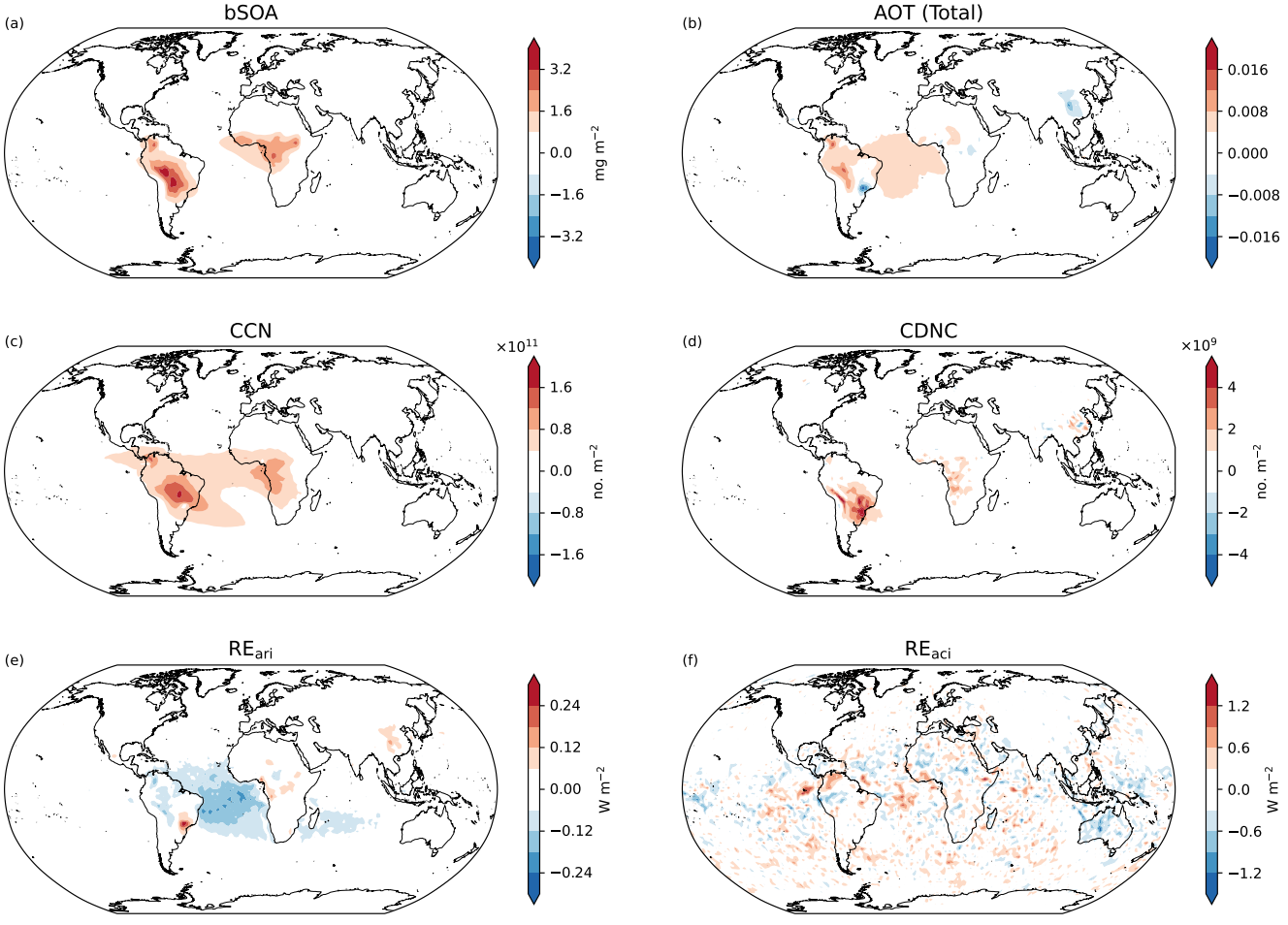

Figure 9. Absolute changes in atmospheric states resulting from restoring present-day grazing land. Maps show variations in; (a) bSOA column mass, (b) total aerosol optical thickness (AOT), (c) cloud condensation nuclei (CCN), (d) cloud droplet number concentration (CDNC), (d) aerosol radiative effect, and (e) cloud radiative effect.

Table 1 outlines the changes in vegetation and atmospheric variables in the two land cover scenarios considered in this study: present-day land cover versus natural vegetation (DCGL-PNV), representing deforestation, and restoration of grazing land versus present-day land cover (DCL-DCGL), representing reforestation. The results indicate that both deforestation of natural vegetation to the present-day land cover, and reforestation of present-day grazing lands significantly impact vegetation and atmospheric variables.

https://doi.org/10.5194/egusphere-2024-2014
Preprint. Discussion started: 12 July 2024

	DCGL−PNV		DCL−DCGL	
	Abs.	Rel.	Abs.	Rel.
Tree cover	−1026 Mha	−18%	+600 Mha	+13%
Veg. Biomass	−64 PgC	−11%	+43 PgC	+9%
Isoprene	−224.8 Tg	−27%	+140.4 Tg	+23%
Monoterpenes	−18.7 Tg	−25%	+11.6 Tg	+20%
bSOA	−0.16 Tg	−29.0%	+0.11 Tg	+25.7%
OA	−0.17 Tg	−9.3%	+0.12 Tg	+6.3%
AOT(OC)	-8.0×10^{-4}	−7%	$+4.4 \times 10^{-4}$	+3.8%
AOT(Total)	-3.0×10^{-4}	−0.5%	$+2.5 \times 10^{-4}$	+0.3%
CCN	-2.6×10^{10} no. m^{-3}	−4.8%	$+1.7 \times 10^{10}$ no. m^{-3}	+3.5%
CDNC	-4.7×10^{7} no. m^{-3}	−0.2%	$+3.3 \times 10^{7}$ no. m^{-3}	+0.2%
RE_{ari}	+60.4 mW m^{-2}	+2.2%	−38.2 mW m^{-2}	−1.4%
RE_{aci}	−8.7 mW m^{-2}	−0.002%	+1.6 mW m^{-2}	+0.002%

Table 1. Changes in vegetation and atmospheric variables for the two land cover scenarios: present-day land cover vs. natural vegetation (DCGL−PNV) and restoration of grazing land vs. present-day land cover (DCL−DCGL). Tree cover, vegetation biomass, isoprene, monoterpenes, bSOA, and OA are global yearly sums, while AOT, CCN, CDNC, and RE, are global yearly means.

4 Discussion

The present study offers insights into the ongoing impact of human-induced deforestation and potential reforestation on atmospheric aerosols, building upon existing literature. Consistent with prior research documenting significant reductions in global vegetation due to human land use changes, our simulations confirm a substantial decline in tree cover and vegetation biomass, i.e., in carbon storage, as a result of deforestation. Hu et al. (2021) estimates that between 1992 and 2018, 722 Mha of forests were converted into agricultural land, while, Bhan et al. (2022) estimates the terrestrial biosphere's global carbon stock for the year 1950 to be 450 PgC. These estimates agree with the values simulated bt LPJ-GUESS and suggest that the changes in the biosphere due to land use change simulated in this study are consistent with earlier work.

4.1 BVOC emissions changes

Studies agree that land use changes predominantly affect BVOC emissions through the expansion of croplands in tropical regions such as the Amazon, central Africa, and Southeast Asia (Szogs et al., 2017). For example, Lathière et al. (2006) show a reduction of approximately 24% in isoprene emissions between 1901 and 2002. Additionally, Unger (2014) reports that land cover changes from the 1850s to the 2000s resulted in a global decrease of approximately 35% in BVOC emissions. In a comprehensive literature review exploring the influence of Land Use and Land Cover Change (LULCC) on atmospheric composition and climate, it was estimated that from the preindustrial era to the present, LULCC has led to a decrease of 15-

https://doi.org/10.5194/egusphere-2024-2014
Preprint. Discussion started: 12 July 2024

36% in global isoprene emissions (Heald and Spracklen, 2015). Scott et al. (2018) reports a global decrease in isoprene and monoterpenes emissions of 87% and 94%, respectively, resulting from complete global deforestation. The 26% decrease in BVOC emissions reported in this study is in line with the findings reported in the literature, particularly because many studies analyse changes from preindustrial times, while our work focuses on changes from human land use compared to natural vegetation.

The global yearly isoprene and monoterpene emission budgets from this study are relatively high compared to other global estimates in the literature, as shown in Vella et al. (2023a). Some atmospheric chemistry studies using MEAGN in EMAC, e.g., Pozzer et al. (2022b), employ a global scaling factor to dampen the global emissions to desired values. However, in this study, no scaling factors were applied, which means that the values reported here may be slightly overestimated.

4.2 Aerosol burden

The rapid oxidation of BVOC, yields oxygenated intermediate species near the surface, which act as precursors for the formation of bSOA. This explains the high abundance of bSOA in the lower atmosphere (see vertical profiles in Fig. 4). As bSOA is dispersed in the atmosphere, concentrations typically decrease due to mixing and dilution. However, the vertical profile of bSOA is also governed by the vapour pressure of the oxygenated intermediates, which decreases with lower temperatures as they ascend in the troposphere. When they are transported upward, the reduced volatility at lower temperatures prompts the transition of oxygenated intermediates into the aerosol phase, contributing to the formation of bSOA. Consequently, this interplay between oxidation, transport, and vapour pressure-driven processes imparts a distinctive D-shaped vertical profile of biogenic SOA concentrations, with elevated concentrations near the surface, followed by an increase in bSOA towards higher altitudes, and ultimately a decline in the upper atmosphere. In the low latitudes (tropics), the D-shape in bSOA concentration is only faint (Fig. 4e). The prevalence of warm air, relatively high boundary layers, and the occurrence of deep convection transporting both aerosol particles as well as precursors into the upper troposphere lead to the maximum gas-to-particle partitioning occurring at higher altitudes, typically around 100-200 hPa, resulting in a secondary local upper tropospheric enhancement.

Several studies estimate the global mean burden bSOA at ∼0.5-0.77 Tg (Henze et al., 2008; Pye et al., 2010; Hoyle et al., 2007; Tsigaridis and Kanakidou, 2007; Tilmes et al., 2019). This indicates that in the present-day deforestation scenario, ORACLE provides a lower estimate of bSOA burden (0.40 Tg) compared to literature values. Pozzer et al. (2022a) evaluated OA from ORACLE in EMAC and found that surface concentrations are well represented, however, OA is strongly underestimated in the free troposphere. The work from Pozzer et al. (2022a) employed the Mainz Organic Mechanism (MOM), which is a more complex chemical mechanism compared to the one used in this study (i.e., the Mainz Isoprene Mechanism, MIM), nevertheless, this indicates that even with a more complex mechanism EMAC calculates a lower OA globally. Heald and Geddes (2016) reports a global annual mean tropospheric burden of bSOA to decrease by 13% due to land use change between 1850 and 2000, while Scott et al. (2018) estimates a 91% decrease in SOA from simulated global deforestation. Our model calculations suggest a reduction of approximately 30% in bSOA from crop and grazing land deforestation compared to natural vegetation.

Regionally, the derived total AOT exhibits opposing effects, particularly, pockets of increased total AOT are evident in confined regions and notably in Southeast (SE) Asia (Fig. 5e). Here, the extinction from H2O and WASO is found to be increasing,

https://doi.org/10.5194/egusphere-2024-2014
Preprint. Discussion started: 12 July 2024

effectively masking the expected reduction in OA extinction from lower BVOC precursors in DCGL. This phenomenon is linked to the growth of aerosol particles into what is commonly referred to as the "Greenfield gap" - a range characterised by lower deposition velocities and scavenging values (Greenfield, 1957). This growth adds to the burden of WASO compounds and their associated water uptake, thereby amplifying aerosol extinction. Moreover, the absence of organics exacerbates this effect, leading to a disproportionate condensation on accumulation mode particles at the expense of Aitken mode particles. Consequently, the increased presence of water soluble compounds, coupled with increased aerosol water content and a shift in size distribution towards larger particles, collectively contribute to the observed increase in extinction in these specific areas. Nevertheless, plotting the relative difference of total AOT (Fig. S6b) shows that this effect is not very prominent, with an increase in AOT in this region of less than 4%.

4.3 Cloud properties and radiative effects

Studies focusing on changes in cloud properties due to perturbed BVOC precursors and SOA loading resulting from land use change are limited. Changes in cloud properties are often considered as the indirect radiative effect of aerosol-cloud interactions. Scott et al. (2014) investigated the impact of bSOA on CCN and CDNC in the present-day atmosphere, and found that bSOA increases the mean annual concentration of CCN by 3.6–21.1%, and the global annual mean concentration of CDNC by 1.9–5.2%. In this work, we show that present-day deforestation, when compared to the potential vegetation scenario, yields a decrease of 4.8% in CCN, but only a small decrease of 0.2% in CDNC, with a slightly more prominent reduction of 0.6% over tropical regions. The most significant change in cloud droplet count occurs over the Amazon, with an approximate 8% decrease in this region (Fig. S7d). This suggests that the changes in CCN resulting from deforestation align well with findings from Scott et al. (2018). The changes in CDNC simulated by EMAC, however, seem to be very localised, in particular over the Amazon rain forest, but the global impact on CDNC is small. Deforestation-induced changes in CDNC are less than 10% over the Amazon and less than 1% globally (Fig. S6 and S7). It is worth pointing out that the effect on cloud droplet numbers reported here only stems from aerosol-cloud interactions. In reality, reduced tree cover may lead to less evapotranspiration, which modifies the Bowen ratio (sensible to latent heat ratio) and potentially influences the cloud effect, however, this feedback is suppressed in our simulations. Additionally, in this model setup, only aerosol-cloud interactions with large-scale clouds are considered. Therefore, the impact of changes in the aerosol burden on convective clouds and their potential radiative effects are not captured.

Biogenic SOA is known to have net cooling effects on the Earth's climate by scattering a portion of incoming solar radiation back into space (Tilmes et al., 2019). Therefore, changes in aerosol numbers and composition from deforestation result in net warming from the lack of aerosol scattering, while reforestation leads to the opposite effect with a net cooling effect (Fig. 7a and Fig. 9e). Scott et al. (2018) showed that full deforestation leads to a radiative effect of 117 mW m^{-2} attributed to aerosols and 200 mW m^{-2} attributed to clouds. However, deforestation projected for 2100 under the RCP8.5 scenario yields only 6 mW m^{-2} of radiative effects attributed to aerosols, with negligible indirect effects from clouds. O'Donnell et al. (2011) shows a total SOA direct effect of 310 mW m^{-2}. The comparatively small direct aerosol effect reported here from deforestation relative to the PNV scenario (60.4 mW m^{-2}) may stem from differences in methodology compared to other studies, which focus on

https://doi.org/10.5194/egusphere-2024-2014
Preprint. Discussion started: 12 July 2024

the effects of full deforestation or total SOA (not bSOA). However, our RE_{ari} estimates might be underestimating the actual impact due to comparatively lower bSOA budgets in our model runs.

For the afforestation scenario, we acknowledge that this is an idealistic sensitivity analysis, perturbing only the land use cover while maintaining present-day values for greenhouse gas concentrations and anthropogenic emissions. In different future scenarios, these key variables would play a crucial role in determining aerosol behaviour radiative effects. This is also highlighted in this study, where we showed that over Southeast Asia, where anthropogenic aerosols are present in relatively high numbers, the reduction in global OA from deforestation resulted in changes in the aerosol-size distribution over this area leading to an opposing effect in aerosol extinction.

In separate analyses assessing the statistical significance of atmospheric state changes resulting from deforestation, we found that changes in BVOC emissions and bSOA column mass exhibit statistically significant changes with 95% confidence (two-tailed Student's t-test, i.e. $p<0.05$). Similarly, variations in AOT attributed to OA and total aerosol also indicated statistical significance. However, changes in CCN, CDNC, and cloud radiative effect did not demonstrate statistical significance attributed to deforestation. The aerosol radiative effect from deforestation did show statistical significance with 85% confidence, well over one sigma (68.27%) over the tropical Atlantic Ocean. While some studies, such as those employing the UK Earth System Model (UKESM) and the Community Earth System Model (CESM2), indicate statistically significant direct radiative effects from deforestation at a 95% confidence level (Weber et al., 2024), other studies, such as the one from Unger (2014), employing the Yale-E2 global carbon–chemistry-climate model, suggest that the global-scale impacts of cropland expansion on bSOA are not statistically significant relative to interannual variability in climate. We argue that the land cover changes assessed in this study significantly impact biogenic aerosol budgets. However, it appears that the influence on global aerosols and subsequent effects on cloud properties and radiative effects on a global scale are likely to be minor.

5 Conclusions

Understanding how land use changes alter atmospheric composition is crucial for grasping the impact of human activities on the Earth system, both past and future. This study presents a comprehensive evaluation of two land-use scenarios, focusing on how changes in BVOC emissions influence the atmosphere and climate. We find that present-day deforestation results in a 73% decrease in isoprene emissions and a 75% decrease in monoterpene emissions. Consequently, the bSOA burden decreases from 0.56 Tg to 0.40 Tg, and the total OA burden decreases from 1.80 Tg to 1.70 Tg. As expected, this leads to a reduction in OC extinction, especially in the tropics near the source of bSOA and its precursors. Upon examining the impact on total aerosol extinction, the model indicates declines in AOT over South America and the tropical Atlantic Ocean. However, aerosol extinction increases over SE Asia in the present-day deforestation scenario compared to PNV conditions. Particularly in SE Asia, the reduction in organic material results in the growth of water-soluble organic compounds (WASO). The absence of organics leads to more condensation on accumulation mode particles and less condensation on Aitken mode particles, resulting in increased aerosol water uptake and a shift in the aerosol size distribution towards larger particles. This effectively increases aerosol extinction.

https://doi.org/10.5194/egusphere-2024-2014
Preprint. Discussion started: 12 July 2024

The perturbations in aerosols resulting from deforestation lead to a positive radiative effect in the tropics (warming), stemming from the reduced aerosol burden. The increased presence of WASO compounds over SE Asia contributes to a negative radiative effect (cooling) in this region. However, our findings indicate a global positive radiative effect of 60.4 mW m^{-2} (aerosol + cloud). In the reforestation scenario, isoprene and monoterpenes fluxes increase by 23% and 20% respectively, leading to an increase in the bSOA burden by 0.23 Tg and a negative radiative effect of 38.2 mW m^{-2}.

Data availability. *Will be made available on Zenodo*

Author contributions. RV, HT, and MF implemented and tested the deforestation routine. RV prepared the model setup and performed the simulations with inputs from HT, AT, and AP. AT provided technical assistance for ORACLE and provided scripts to handle its output. RV evaluated the simulations, analysed the model results and wrote the article. The results were interpreted by all co-authors, with a special focus on vegetation analysis provided by MF and TH. JL and HT supervised the project. All authors discussed the results and contributed to the review and editing of the paper.

Competing interests. At least one of the (co-)authors is a member of the editorial board of *Atmospheric Chemistry and Physics*.

Acknowledgements. The model simulations have been performed at the German Climate Computing Centre (DKRZ) through support from the Max Planck Society and the JGU Mainz. This work was supported by the Max Planck Graduate Center with the Johannes Gutenberg-Universität Mainz (MPGC). AP acknowledge the European Commission Horizon Europe project FOCI (Grant Agreement No 101056783).

https://doi.org/10.5194/egusphere-2024-2014
Preprint. Discussion started: 12 July 2024

References

Abdul-Razzak, H. and Ghan, S. J.: A parameterization of aerosol activation: 2. Multiple aerosol types, Journal of Geophysical Research: Atmospheres, 105, 6837–6844, https://doi.org/https://doi.org/10.1029/1999JD901161, 2000.

Alessandri, A., Catalano, F., De Felice, M., Van Den Hurk, B., Reyes, F. D., Boussetta, S., Balsamo, G., and Miller, P. A.: Multi-scale enhancement of climate prediction over land by increasing the model sensitivity to vegetation variability in EC-Earth, Climate dynamics, 49, 1215–1237, 2017.

Atkinson, R.: Atmospheric chemistry of VOCs and NOx, Atmospheric environment, 34, 2063–2101, 2000.

Atkinson, R. and Arey, J.: Gas-phase tropospheric chemistry of biogenic volatile organic compounds: a review, Atmospheric Environment, 37, 197–219, 2003.

Betts, R., Cox, P., Collins, M., Harris, P., Huntingford, C., and Jones, C.: The role of ecosystem-atmosphere interactions in simulated Amazonian precipitation decrease and forest dieback under global climate warming, Theoretical and applied climatology, 78, 157–175, 2004.

Bhan, M., Meyfroidt, P., Matej, S., Erb, K.-H., and Gingrich, S.: A mid-20th century inventory-based estimate of global terrestrial vegetation carbon stocks, Journal of Land Use Science, 17, 429–453, 2022.

Bonan, G. B.: Forests and climate change: forcings, feedbacks, and the climate benefits of forests, science, 320, 1444–1449, 2008.

Brinkop, S. and Roeckner, E.: Sensitivity of a general circulation model to parameterizations of cloud–turbulence interactions in the atmospheric boundary layer, Tellus A, 47, 197–220, 1995.

Chen, Q., Farmer, D., Schneider, J., Zorn, S., Heald, C., Karl, T., Guenther, A., Allan, J., Robinson, N., Coe, H., et al.: Mass spectral characterization of submicron biogenic organic particles in the Amazon Basin, Geophysical Research Letters, 36, 2009.

de Sá, S. S., Rizzo, L. V., Palm, B. B., Campuzano-Jost, P., Day, D. A., Yee, L. D., Wernis, R., Isaacman-VanWertz, G., Brito, J., Carbone, S., et al.: Contributions of biomass-burning, urban, and biogenic emissions to the concentrations and light-absorbing properties of particulate matter in central Amazonia during the dry season, Atmospheric Chemistry and Physics, 19, 7973–8001, 2019.

Dee, D. P., Uppala, S. M., Simmons, A. J., Berrisford, P., Poli, P., Kobayashi, S., Andrae, U., Balmaseda, M., Balsamo, G., Bauer, d. P., et al.: The ERA-Interim reanalysis: Configuration and performance of the data assimilation system, Quarterly Journal of the royal meteorological society, 137, 553–597, 2011.

Donahue, N. M., Robinson, A., Stanier, C., and Pandis, S.: Coupled partitioning, dilution, and chemical aging of semivolatile organics, Environmental science & technology, 40, 2635–2643, 2006.

Field, C. B. and Raupach, M. R.: The global carbon cycle: integrating humans, climate, and the natural world, vol. 62, Island Press, 2004.

Forrest, M., Tost, H., Lelieveld, J., and Hickler, T.: Including vegetation dynamics in an atmospheric chemistry-enabled general circulation model: linking LPJ-GUESS (v4. 0) with the EMAC modelling system (v2. 53), Geoscientific Model Development, 13, 1285–1309, 2020.

Forster, P., Ramaswamy, V., Artaxo, P., Berntsen, T., Betts, R., Fahey, D. W., Haywood, J., Lean, J., Lowe, D. C., Myhre, G., Nganga, J., Prinn, R., Raga, G., Schulz, M., and Van Dorland, R.: Changes in Atmospheric Constituents and in Radiative Forcing, in: Climate Change 2007: The Physical Science Basis. Contribution of Working Group I to the Fourth Assessment Report of the Intergovernmental Panel on Climate Change, edited by Solomon, S., Qin, D., Manning, M., Chen, Z., Marquis, M., Averyt, K. B., Tignor, M., and Miller, H. L., Cambridge University Press, Cambridge, United Kingdom and New York, NY, USA, 2007a.

https://doi.org/10.5194/egusphere-2024-2014
Preprint. Discussion started: 12 July 2024

Forster, P., Ramaswamy, V., Artaxo, P., Berntsen, T., Betts, R., Fahey, D. W., Haywood, J., Lean, J., Lowe, D. C., Myhre, G., et al.: Changes in atmospheric constituents and in radiative forcing, Climate Change 2007: The Physical Science Basis. Contribution of Working Group I to the 4th Assessment Report of the Intergovernmental Panel on Climate Change, 2007b.

Ghan, S. J.: Estimating aerosol effects on cloud radiative forcing, Atmospheric Chemistry and Physics, 13, 9971–9974, 2013.

Greenfield, S. M.: Rain scavenging of radioactive particulate matter from the atmosphere, Journal of Atmospheric Sciences, 14, 115–125, 1957.

Guenther, A., Hewitt, C. N., Erickson, D., Fall, R., Geron, C., Graedel, T., Harley, P., Klinger, L., Lerdau, M., McKay, W., et al.: A global model of natural volatile organic compound emissions, Journal of Geophysical Research: Atmospheres, 100, 8873–8892, 1995.

Guenther, A., Karl, T., Harley, P., Wiedinmyer, C., Palmer, P. I., and Geron, C.: Estimates of global terrestrial isoprene emissions using MEGAN (Model of Emissions of Gases and Aerosols from Nature), Atmospheric Chemistry and Physics, 6, 3181–3210, 2006.

Guenther, A. B., Zimmerman, P. R., Harley, P. C., Monson, R. K., and Fall, R.: Isoprene and monoterpene emission rate variability: model evaluations and sensitivity analyses, Journal of Geophysical Research: Atmospheres, 98, 12 609–12 617, 1993.

Heald, C. L. and Geddes, J. A.: The impact of historical land use change from 1850 to 2000 on secondary particulate matter and ozone, Atmospheric Chemistry and Physics, 16, 14 997–15 010, 2016.

Heald, C. L. and Spracklen, D. V.: Land use change impacts on air quality and climate, Chemical reviews, 115, 4476–4496, 2015.

Henze, D., Seinfeld, J., Ng, N., Kroll, J., Fu, T.-M., Jacob, D. J., and Heald, C.: Global modeling of secondary organic aerosol formation from aromatic hydrocarbons: high-vs. low-yield pathways, Atmospheric Chemistry and Physics, 8, 2405–2420, 2008.

Hewitt, C., Lee, J., MacKenzie, A., Barkley, M., Carslaw, N., Carver, G., Chappell, N., Coe, H., Collier, C., Commane, R., et al.: Overview: oxidant and particle photochemical processes above a south-east Asian tropical rainforest (the OP3 project): introduction, rationale, location characteristics and tools, Atmospheric Chemistry and Physics, 10, 169–199, 2010.

Hoyle, C., Berntsen, T., Myhre, G., and Isaksen, I.: Secondary organic aerosol in the global aerosol–chemical transport model Oslo CTM2, Atmospheric Chemistry and Physics, 7, 5675–5694, 2007.

Hu, X., Næss, J. S., Iordan, C. M., Huang, B., Zhao, W., and Cherubini, F.: Recent global land cover dynamics and implications for soil erosion and carbon losses from deforestation, Anthropocene, 34, 100 291, 2021.

Hurtt, G. C., Chini, L. P., Frolking, S., Betts, R., Feddema, J., Fischer, G., Fisk, J., Hibbard, K., Houghton, R., Janetos, A., et al.: Harmonization of land-use scenarios for the period 1500–2100: 600 years of global gridded annual land-use transitions, wood harvest, and resulting secondary lands, Climatic change, 109, 117–161, 2011.

Jöckel, P., Sander, R., Kerkweg, A., Tost, H., and Lelieveld, J.: the modular earth submodel system (MESSy)-a new approach towards earth system modeling, Atmospheric Chemistry and Physics, 5, 433–444, 2005.

Jöckel, P., Tost, H., Pozzer, A., Brühl, C., Buchholz, J., Ganzeveld, L., Hoor, P., Kerkweg, A., Lawrence, M., Sander, R., et al.: The atmospheric chemistry general circulation model ECHAM5/MESSy1: consistent simulation of ozone from the surface to the mesosphere, Atmospheric Chemistry and Physics, 6, 5067–5104, 2006.

Jöckel, P., Tost, H., Pozzer, A., Kunze, M., Kirner, O., Brenninkmeijer, C. A., Brinkop, S., Cai, D. S., Dyroff, C., Eckstein, J., et al.: Earth system chemistry integrated modelling (ESCiMo) with the modular earth submodel system (MESSy) version 2.51, Geoscientific Model Development, 9, 1153–1200, 2016.

Jokinen, T., Berndt, T., Makkonen, R., Kerminen, V.-M., Junninen, H., Paasonen, P., Stratmann, F., Herrmann, H., Guenther, A. B., Worsnop, D. R., et al.: Production of extremely low volatile organic compounds from biogenic emissions: Measured yields and atmospheric implications, Proceedings of the National Academy of Sciences, 112, 7123–7128, 2015.

https://doi.org/10.5194/egusphere-2024-2014
Preprint. Discussion started: 12 July 2024

Kavouras, I. G., Mihalopoulos, N., and Stephanou, E. G.: Formation of atmospheric particles from organic acids produced by forests, Nature, 395, 683–686, 1998.

Kerkweg, A., Sander, R., Tost, H., and Jöckel, P.: Implementation of prescribed (OFFLEM), calculated (ONLEM), and pseudo-emissions (TNUDGE) of chemical species in the Modular Earth Submodel System (MESSy), Atmospheric Chemistry and Physics, 6, 3603–3609, 2006.

Klein Goldewijk, K., Beusen, A., Doelman, J., and Stehfest, E.: Anthropogenic land use estimates for the Holocene–HYDE 3.2, Earth System Science Data, 9, 927–953, 2017.

Lathière, J., Hauglustaine, D. A., Friend, A. D., De Noblet-Ducoudré, N., Viovy, N., and Folberth, G. A.: Impact of climate variability and land use changes on global biogenic volatile organic compound emissions, Atmospheric Chemistry and Physics, 6, 2129–2146, https://doi.org/10.5194/acp-6-2129-2006, 2006.

Lelieveld, J. a., Butler, T. M., Crowley, J. N., Dillon, T. J., Fischer, H., Ganzeveld, L., Harder, H., Lawrence, M. G., Martinez, M., Taraborrelli, D., et al.: Atmospheric oxidation capacity sustained by a tropical forest, Nature, 452, 737–740, 2008.

Lohmann, U. and Ferrachat, S.: Impact of parametric uncertainties on the present-day climate and on the anthropogenic aerosol effect, Atmospheric Chemistry and Physics, 10, 11 373–11 383, 2010.

Lohmann, U. and Kärcher, B.: First interactive simulations of cirrus clouds formed by homogeneous freezing in the ECHAM general circulation model, Journal of Geophysical Research: Atmospheres, 107, AAC–8, 2002.

Lohmann, U., Feichter, J., Chuang, C. C., and Penner, J. E.: Prediction of the number of cloud droplets in the ECHAM GCM, Journal of Geophysical Research: Atmospheres, 104, 9169–9198, 1999.

Lohmann, U., Stier, P., Hoose, C., Ferrachat, S., Kloster, S., Roeckner, E., and Zhang, J.: Cloud microphysics and aerosol indirect effects in the global climate model ECHAM5-HAM, Atmospheric Chemistry and Physics, 7, 3425–3446, 2007.

Nordeng, E. T.: Extended versions of the convective parametrization scheme at ECMWF and their impact on the mean and transient activity of the model in the tropics., Research Department Technical Memorandum, 206, 1–41, 1994.

O'Donnell, D., Tsigaridis, K., and Feichter, J.: Estimating the direct and indirect effects of secondary organic aerosols using ECHAM5-HAM, Atmospheric Chemistry and Physics, 11, 8635–8659, 2011.

Petters, M. D. and Kreidenweis, S. M.: A single parameter representation of hygroscopic growth and cloud condensation nucleus activity, Atmospheric Chemistry and Physics, 7, 1961–1971, https://doi.org/10.5194/acp-7-1961-2007, 2007.

Pöschl, U., von Kuhlmann, R., Poisson, N., and Crutzen, P. J.: Development and intercomparison of condensed isoprene oxidation mechanisms for global atmospheric modeling, Journal of Atmospheric Chemistry, 37, 29–52, 2000.

Pozzer, A., Reifenberg, S. F., Kumar, V., Franco, B., Kohl, M., Taraborrelli, D., Gromov, S., Ehrhart, S., Jöckel, P., Sander, R., Fall, V., Rosanka, S., Karydis, V., Akritidis, D., Emmerichs, T., Crippa, M., Guizzardi, D., Kaiser, J. W., Clarisse, L., Kiendler-Scharr, A., Tost, H., and Tsimpidi, A.: Simulation of organics in the atmosphere: evaluation of EMACv2.54 with the Mainz Organic Mechanism (MOM) coupled to the ORACLE (v1.0) submodel, Geoscientific Model Development, 15, 2673–2710, https://doi.org/10.5194/gmd-15-2673-2022, 2022a.

Pozzer, A., Reifenberg, S. F., Kumar, V., Franco, B., Kohl, M., Taraborrelli, D., Gromov, S., Ehrhart, S., Jöckel, P., Sander, R., et al.: Simulation of organics in the atmosphere: evaluation of EMACv2. 54 with the Mainz Organic Mechanism (MOM) coupled to the ORACLE (v1. 0) submodel, Geoscientific model development, 15, 2673–2710, 2022b.

Pringle, K., Tost, H., Steil, B., Giannadaki, D., Nenes, A., Fountoukis, C., Stier, P., Vignati, E., Lelieveld, J., et al.: Description and evaluation of GMXe: a new aerosol submodel for global simulations (v1), Geoscientific Model Development, 3, 391–412, 2010.

https://doi.org/10.5194/egusphere-2024-2014
Preprint. Discussion started: 12 July 2024

Pye, H., Chan, A., Barkley, M., and Seinfeld, J.: Global modeling of organic aerosol: the importance of reactive nitrogen (NO x and NO 3), Atmospheric Chemistry and Physics, 10, 11 261–11 276, 2010.

Roeckner, E., Brokopf, R., Esch, M., Giorgetta, M., Hagemann, S., Kornblueh, L., Manzini, E., Schlese, U., and Schulzweida, U.: Sensitivity of simulated climate to horizontal and vertical resolution in the ECHAM5 atmosphere model, Journal of Climate, 19, 3771–3791, 2006.

Sander, R., Baumgaertner, A., Cabrera-Perez, D., Frank, F., Gromov, S., Grooß, J.-U., Harder, H., Huijnen, V., Jöckel, P., Karydis, V. A., et al.: The community atmospheric chemistry box model CAABA/MECCA-4.0, Geoscientific model development, 12, 1365–1385, 2019.

Schmale, J., Schneider, J., Nemitz, E., Tang, Y., Dragosits, U., Blackall, T., Trathan, P., Phillips, G., Sutton, M., and Braban, C.: Sub-Antarctic marine aerosol: dominant contributions from biogenic sources, Atmospheric Chemistry and Physics, 13, 8669–8694, 2013.

Scott, C., Rap, A., Spracklen, D., Forster, P., Carslaw, K., Mann, G., Pringle, K., Kivekäs, N., Kulmala, M., Lihavainen, H., et al.: The direct and indirect radiative effects of biogenic secondary organic aerosol, Atmospheric Chemistry and Physics, 14, 447–470, 2014.

Scott, C. E., Monks, S. A., Spracklen, D., Arnold, S., Forster, P., Rap, A., Äijälä, M., Artaxo, P., Carslaw, K., Chipperfield, M., et al.: Impact on short-lived climate forcers increases projected warming due to deforestation, Nature communications, 9, 157, 2018.

Shrivastava, M., Cappa, C. D., Fan, J., Goldstein, A. H., Guenther, A. B., Jimenez, J. L., Kuang, C., Laskin, A., Martin, S. T., Ng, N. L., et al.: Recent advances in understanding secondary organic aerosol: Implications for global climate forcing, Reviews of Geophysics, 55, 509–559, 2017.

Sindelarova, K., Granier, C., Bouarar, I., Guenther, A., Tilmes, S., Stavrakou, T., Müller, J.-F., Kuhn, U., Stefani, P., and Knorr, W.: Global data set of biogenic VOC emissions calculated by the MEGAN model over the last 30 years, Atmospheric Chemistry and Physics, 14, 9317–9341, 2014.

Smith, B., Prentice, I. C., and Sykes, M. T.: Representation of vegetation dynamics in the modelling of terrestrial ecosystems: comparing two contrasting approaches within European climate space, Global ecology and biogeography, pp. 621–637, 2001.

Smith, B., Wårlind, D., Arneth, A., Hickler, T., Leadley, P., Siltberg, J., and Zaehle, S.: Implications of incorporating N cycling and N limitations on primary production in an individual-based dynamic vegetation model, Biogeosciences, 11, 2027–2054, 2014.

Spracklen, D., Jimenez, J., Carslaw, K., Worsnop, D., Evans, M., Mann, G., Zhang, Q., Canagaratna, M., Allan, J., Coe, H., et al.: Aerosol mass spectrometer constraint on the global secondary organic aerosol budget, Atmospheric Chemistry and Physics, 11, 12 109–12 136, 2011.

Szogs, S., Arneth, A., Anthoni, P., Doelman, J. C., Humpenöder, F., Popp, A., Pugh, T. A., and Stehfest, E.: Impact of LULCC on the emission of BVOCs during the 21st century, Atmospheric Environment, 165, 73–87, 2017.

Tiedtke, M.: A comprehensive mass flux scheme for cumulus parameterization in large-scale models, Monthly weather review, 117, 1779–1800, 1989.

Tiitta, P., Vakkari, V., Croteau, P., Beukes, J., Van Zyl, P., Josipovic, M., Venter, A., Jaars, K., Pienaar, J., Ng, N., et al.: Chemical composition, main sources and temporal variability of PM 1 aerosols in southern African grassland, Atmospheric Chemistry and Physics, 14, 1909–1927, 2014.

Tilmes, S., Hodzic, A., Emmons, L., Mills, M., Gettelman, A., Kinnison, D. E., Park, M., Lamarque, J.-F., Vitt, F., Shrivastava, M., et al.: Climate forcing and trends of organic aerosols in the Community Earth System Model (CESM2), Journal of Advances in Modeling Earth Systems, 11, 4323–4351, 2019.

Tost, H., Jöckel, P., Kerkweg, A., Sander, R., and Lelieveld, J.: A new comprehensive SCAVenging submodel for global atmospheric chemistry modelling, Atmospheric Chemistry and Physics, 6, 565–574, 2006a.

https://doi.org/10.5194/egusphere-2024-2014
Preprint. Discussion started: 12 July 2024

Tost, H., Jöckel, P., and Lelieveld, J.: Influence of different convection parameterisations in a GCM, Atmospheric Chemistry and Physics, 6, 5475–5493, 2006b.

Tsigaridis, K. and Kanakidou, M.: Secondary organic aerosol importance in the future atmosphere, Atmospheric Environment, 41, 4682–4692, 2007.

Tsimpidi, A., Karydis, V., Pozzer, A., Pandis, S., and Lelieveld, J.: ORACLE (v1. 0): module to simulate the organic aerosol composition and evolution in the atmosphere, Geoscientific Model Development, 7, 3153–3172, 2014.

Tsimpidi, A. P., Karydis, V. A., Pandis, S. N., and Lelieveld, J.: Global combustion sources of organic aerosols: model comparison with 84 AMS factor-analysis data sets, Atmospheric Chemistry and Physics, 16, 8939–8962, 2016.

Tsimpidi, A. P., Karydis, V. A., Pandis, S. N., and Lelieveld, J.: Global-scale combustion sources of organic aerosols: sensitivity to formation and removal mechanisms, Atmospheric Chemistry and Physics, 17, 7345–7364, 2017.

Tsimpidi, A. P., Karydis, V. A., Pozzer, A., Pandis, S. N., and Lelieveld, J.: ORACLE 2-D (v2. 0): an efficient module to compute the volatility and oxygen content of organic aerosol with a global chemistry–climate model, Geoscientific Model Development, 11, 3369–3389, 2018.

Unger, N.: Human land-use-driven reduction of forest volatiles cools global climate, Nature Climate Change, 4, 907–910, 2014.

Vella, R., Forrest, M., Lelieveld, J., and Tost, H.: Isoprene and monoterpene simulations using the chemistry-climate model EMAC (v2.55) with interactive vegetation from LPJ-GUESS (v4.0), Geoscientific Model Development, 16, 885–906, 2023a.

Vella, R., Pozzer, A., Forrest, M., Lelieveld, J., Hickler, T., and Tost, H.: Changes in biogenic volatile organic compound emissions in response to the El Niño–Southern Oscillation, Biogeosciences, 20, 4391–4412, 2023b.

Vicente-Serrano, S. M., Van der Schrier, G., Beguería, S., Azorin-Molina, C., and Lopez-Moreno, J.-I.: Contribution of precipitation and reference evapotranspiration to drought indices under different climates, Journal of Hydrology, 526, 42–54, 2015.

Weber, J., King, J. A., Abraham, N. L., Grosvenor, D. P., Smith, C. J., Shin, Y. M., Lawrence, P., Roe, S., Beerling, D. J., and Martin, M. V.: Chemistry-albedo feedbacks offset up to a third of forestation's CO2 removal benefits, Science, 383, 860–864, 2024.

Weiss, M., Miller, P. A., van den Hurk, B. J., van Noije, T., Ştefănescu, S., Haarsma, R., Van Ulft, L. H., Hazeleger, W., Le Sager, P., Smith, B., et al.: Contribution of dynamic vegetation phenology to decadal climate predictability, Journal of Climate, 27, 8563–8577, 2014.

Zhang, Q., Parworth, C., Lechner, M., and Jimenez, J.: Aerosol Mass Spectrometer Global Database, https://sites.google.com/site/amsglobaldatabase, https://doi.org/10.6084/m9.figshare.3486719, 2010.